Deformation-softening in ultrafine-grained materials

Jenő Gubicza and Nguyen Quang Chinh

Department of Materials Physics, Eötvös Loránd University, Budapest, Hungary

Email: jeno.gubicza@ttk.elte.hu

Abstract. Plastic deformation is conventionally considered as a route for strengthening of metallic materials. During plastic straining, different crystal defects, such as dislocations, stacking faults and grain boundaries form, hardening the material. On the other hand, plastic deformation may also cause unexpected softening in ultrafine-grained and nanocrystalline materials. This paper summarizes the existing knowledge on this deformation-softening effect.

1. Introduction

Plastic deformation of metals and alloys at room temperature (RT) is usually accompanied by strain hardening, i.e., the true stress increases with increasing true strain [1]. This effect can be used for strengthening of metallic materials. The enhancement of the flow stress during plastic deformation is caused by the increase of the density of lattice defects, such as dislocations and stacking/twin faults [1]. For instance, in face centered cubic (fcc) metals deformed plastically to a strain of about 0.2 at RT, the dislocation density increased to an order of magnitude of 10^{14} m^{-2} [2]. The higher the applied strain, the higher the defect density formed during plastic deformation. Therefore, in the last decades numerous new techniques were developed for achieving large plastic strains in metals in order to obtain high strength materials. These procedures are referred to as severe plastic deformation (SPD) methods [3].

SPD techniques can achieve large plastic strains (higher than one) in metallic materials without significant change of the dimensions of the specimens. The most frequently used SPD methods are Accumulative Roll Bonding (ARB), Equal Channel Angular Pressing (ECAP) and High Pressure Torsion (HPT) [3]. Applying these techniques, the dislocation density saturates at the equivalent strain of about 1-4. The saturation dislocation density of SPD-processed materials varies between 10^{14}-10^{16} m^{-2} [4]. In addition, the grain size is refined below 1 μm due to SPD, resulting in homogeneous ultrafine-grained (UFG) or nanocrystalline microstructures with high yield strength. In the saturation state, the yield strength of SPD-processed metallic materials is one-two orders of magnitude higher than that for coarse-grained counterparts [4].

Recently, it was revealed that plastic deformation may cause softening in UFG and nanocrystalline materials (e.g., see [5,6]). In this paper, this unusual phenomenon referred to as deformation-induced softening (or simply deformation-softening) is overviewed. The research results obtained in this field can be categorized into three classes. In the first case, the deformation-softening was observed during straining of UFG materials formerly annealed at moderate temperatures. The preliminary annealing caused hardening and then subsequent plastic deformation resulted in softening. In the second class of deformation-softening phenomena, the effect was observed for fine-grained materials having low melting points. In the third case, the as-processed defect structure is decayed due to plastic deformation,

thereby causing softening. Accordingly, in the following the results for deformation-softening will be overviewed in three separate sections.

2. Deformation-softening due to plastic straining of anneal-hardened UFG materials

It has been shown recently that annealing of UFG and nanocrystalline materials at moderate temperatures can further enhance the high yield strength achieved due to the formation of the very small grain size [7-13]. This effect is referred to as anneal-hardening which can be observed if the temperature of annealing is only about 0.35-0.45 × T_m where T_m is the melting point, and the duration of heat treatment is short, typically not longer than 1 hour. Anneal-hardening can yield a 10-120% increase of hardness or yield strength, depending on the chemical composition and the microstructure of the material before heat treatment. The application of a moderate annealing temperature prevents the fine-grained microstructure from recrystallization, and only a relaxation of the defect structure occurs. This means that mobile dislocations are annihilated and the remaining dislocations are arranged into low energy agglomerates [7,11]. These effects result in a harder initiation of dislocation glide during plastic deformation after annealing. In addition, the non-equilibrium grain boundaries are relaxed, thereby making the dislocation emission from the boundary more difficult [8,12,13]. The grain boundary relaxation also hinders grain boundary sliding which is an important deformation mechanism in nanocrystalline samples and also in UFG materials with low melting points [14]. In UFG and nanostructured alloys, the segregation of solute elements to grain boundaries can contribute to grain boundary relaxation, yielding a decrease of grain boundary energy [15].

Subsequent plastic deformation after moderate annealing can introduce new mobile dislocations into the relaxed UFG materials, thereby resulting in a lower flow stress (i.e., softening) as demonstrated on Al with 99.2% purity processed by ARB at RT [5,16]. After six cycles of ARB, the yield and ultimate tensile strength values were 259 and 334 MPa, respectively. The elongation to failure was obtained as 7%. The ARB-processed material had an average grain size of about 200 nm with an elongated grain shape. After annealing of the ARB-processed sample at 150 ºC for 30 min, the yield strength increased from 259 to 281 MPa while the ultimate tensile strength was enhanced from 334 to 347 MPa. In addition, the elongation to failure was reduced to 1.4% due to annealing. The effect of anneal-hardening on the ultimate tensile strength and the total elongation are shown in Fig. 1. Then, the annealed sample was cold rolled to the thickness reduction of 15% which led to a decrease of the yield and ultimate tensile strength values to similar values as observed immediately after ARB. In addition, the elongation to failure increased back from 1.4% to about 6.6% (see Fig. 1). The restoration of the softer but ductile behavior due to rolling was explained by the introduction of new mobile dislocations into the anneal-hardened material. The subsequent application of annealing and rolling deformation steps can cause cyclic hardening and softening, respectively, as shown in Fig. 1, i.e., these effects are reversible. This is also valid for the elongation to failure. It is worth noting that the occurrence of deformation-softening depends on the thickness reduction applied in cold rolling [16]. Namely, if the thickness reduction is smaller than about 30% a decrease of strength was observed while above this limit deformation-softening was not observed. The latter phenomenon can be explained by the clustering of dislocations at high rolling strains into configurations causing forest hardening which suppressed the softening effect caused by the newly developed mobile dislocations.

Nanocrystalline high entropy alloys (HEA) also exhibit deformation-softening if the samples first hardened by annealing. This effect was demonstrated on CoCrFeMnNi HEA processed by HPT at RT [17]. It was revealed that annealing at 450 ºC for 1 and 10 h resulted in the development of NiMn, FeCo and Cr nanosized phases which were then dissolved during subsequent deformation in an indentation experiment. This deformation-induced dissolution of the intermetallic phases was most probably caused by the increase of the energy of interfaces between the matrix and the precipitates due to the accumulation of dislocations at these interfaces formed during deformation [17]. The sample subjected to longer annealing (10 h) exhibited a more pronounced decomposition, thus the subsequent deformation caused a higher softening in this material compared to the case of the shorter annealing time (1 h).

Deformation-softening was also observed for nanosized samples, namely for single crystal nanopillars fabricated by ion milling from Au film deposited on a MgO substrate by sputtering [18,19]. The diameter of the Au nanopillars was about 300 nm while their aspect ratio was about two. First, larger nanopillars were pre-strained by compression to the strain of 35%, resulting in the formation of dislocations in the sample which then was re-milled by a focused ion beam. The dislocation density was in the order of 10^{15} m^{-2}. Annealing of these pillars at 260 ºC for 7 min led to an increase of the yield strength which was caused by the development of jogs on dislocations since these jogs hindered the motion of dislocations during further compression. This was a typical anneal-hardening effect. However, vanishing of these jogs was observed during additional compression after annealing, resulting in a decrease of the yield strength to the value observed on the Au nanopillars before the heat treatment.

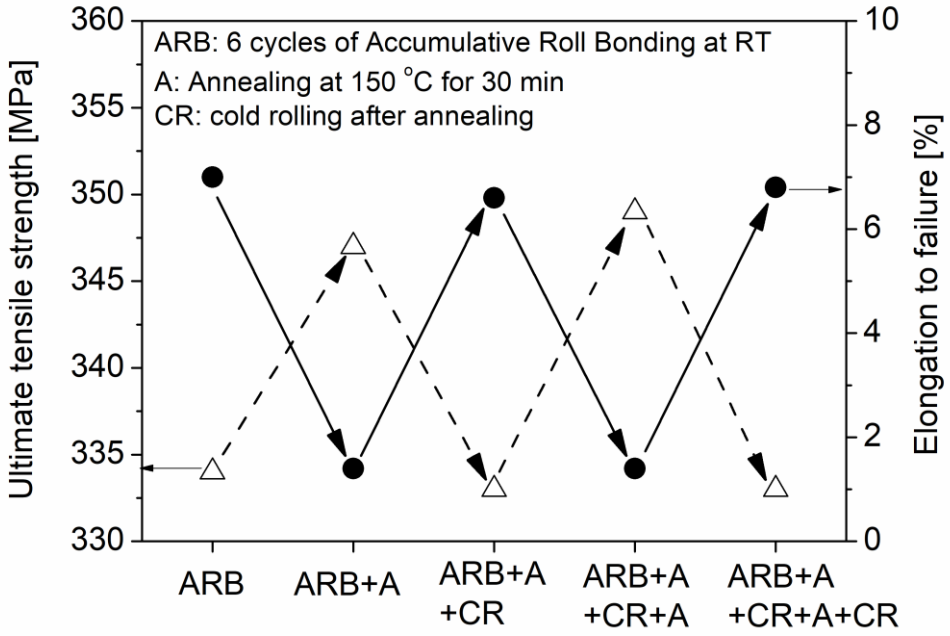

Figure 1. The variation of the ultimate tensile strength and the elongation to failure for ARB-processed Al with 99.2% purity subjected to annealing and rolling cyclically [5,16].

3. Deformation-softening in UFG metals having low melting points

Deformation-softening can also be observed for UFG materials with low melting temperatures [20-25]. In this case, preliminary anneal-hardening is not necessary for the occurrence of softening. The decrease of the yield strength or hardness at RT was observed after SPD-processing of pure metals such as Sn, Pb, In and Zn. For these metals, the melting point varies between 160 and 420 ºC therefore RT corresponds to the homologous temperatures between 0.43 and 0.7. Thus, the grain refinement during SPD yielded an enhanced role of grain boundary sliding in mechanical testing due to the increased amount of grain boundaries even if the test was carried out at RT [26].

The deformation-softening effect was also observed in SPD-processed Al with a slightly higher melting point (660 ºC) but only if the purity exceeded the critical level of 99.9999% (i.e., 6N) [24]. Fig. 2 shows the variation of the hardness as a function of the shear strain schematically for HPT-processed Al with three different purity levels (namely 2N, 4N and 6N purities). For 2N purity Al, the hardness increases monotonously with increasing strain until a saturation state was achieved. This state can be characterized by a dynamic equilibrium between the formation and annihilation of lattice defects such as dislocations and grain boundaries. For 4N purity Al, first the hardness increased but then decreased at high strain values [27,28]. Despite this decrease, the hardness was higher in the steady state achieved

at high strains than that in the initial annealed state. For 6N purity Al, the hardness also increased at low strains but then decreased and the steady state hardness was about 12% smaller than that for the initial annealed material [24]. The hardness reduction at high strains was caused by dynamic recovery and recrystallization which was accompanied by a grain refinement. The steady state grain sizes were 400 nm, 1.3 μm and 20 μm for 2N, 4N and 6N purity Al, respectively. For 4N and 6N purity Al, the hardness was higher at low shear strains (i.e., close to the center of the HPT-processed disks) than that at high strains which can be explained by the larger dislocation density at lower strains. At high strains, the dislocation density strongly decreased due to recrystallization and this softening effect overwhelmed the hardening effect of the smaller grain size, resulting in hardness reduction. It should be emphasized that the hardness of the HPT-processed 6N purity Al sample was lower at high strains than that in the initial annealed state. In the initial material, the grain size was about 1 mm, i.e., about two orders of magnitude higher than that in the steady state for the HPT-processed sample (~20 μm). In the initial large grains, the dislocations formed during hardness testing were stored in the grain interiors (e.g., in cell walls), therefore they contributed to strengthening [24]. At the same time, in the HPT-processed fine-grained sample there is a much larger amount of grain boundaries due to the smaller grain size which acted as sinks of dislocations. In 6N purity Al, dislocations have high mobility due to the high purity level, the relatively low melting point and the high stacking fault energy. Therefore, the dislocations formed during HPT and the subsequent hardness testing can be easily annihilated at grain boundaries, therefore they do not cause hardening. Thus, the HPT-processed 6N Al sample in the steady state is softer than the initial coarse-grained material. It is noted that the contribution of grain boundary sliding to the softening of the HPT-processed 6N Al can not be ruled out as this mechanism was proved to operate during hardness testing of SPD-processed Al even at RT [26].

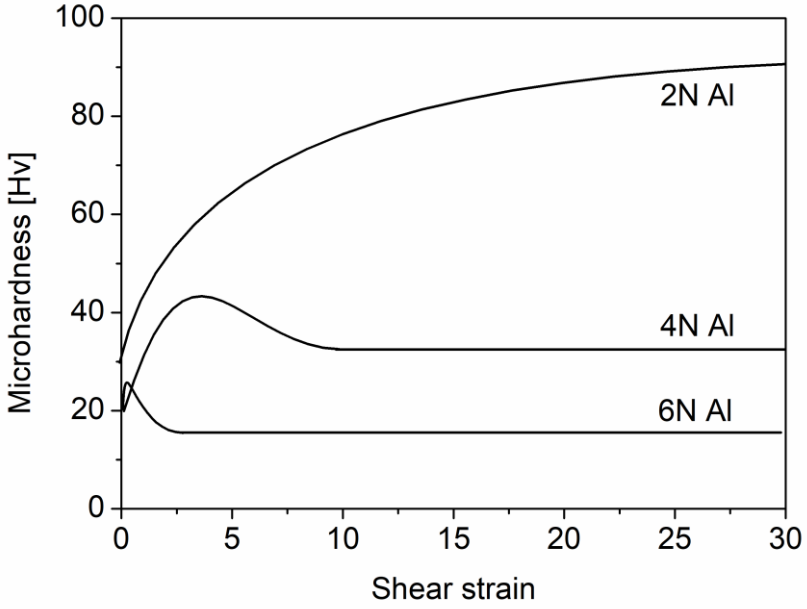

Figure 2. Schematic showing the hardness evolution as a function of shear strain for 2N, 4N and 6N purity Al processed by HPT at RT. The data were taken from [24].

The influence of Zn content on deformation-softening in HPT-processed Al was revealed in a recent study [25]. Al samples with different Zn contents up to 30 wt.% were processed by HPT until the saturation state was achieved, and the microstructure and the mechanical properties were studied as a function of the Zn content. The phase composition in the HPT-processed samples was studied by X-ray diffraction (XRD). The XRD patterns show that the samples contain two phases: the major Al(Zn) and the minor Zn(Al) solid solutions, indicating the decomposition of the initial supersaturated

microstructure. Only the major Al(Zn) phase was studied in detail. Irrespectively of the nominal Zn content, the lattice constant of the Al(Zn) phase was 0.4049 ± 0.0001 nm as determined by XRD which agrees with the lattice parameter of pure Al within the experimental error. The solubility limit of Zn in Al at RT is very low (about 2 wt. % [29]) which can expain the undetectable deviation of the lattice constant from the value of pure Al.

The Zn phase content in the HPT-processed Al-Zn samples was characterized by its intensity fraction in the XRD patterns. This quantity was determined as the ratio of the sum of the areas under the Zn peaks and the sum of the areas under all peaks after background subtraction. This intensity fraction of Zn peaks reflects the Zn precipitate volume fraction (but not equivalent to that). Fig. 3a shows this quantity as a function of the nominal Zn content. It is clear that the Zn phase fraction follows monotonously the nominal Zn content and the values suggest that for high Zn content the majority of Zn atoms are in the Zn phase. This observation is in accordance with the low solubility limit of Zn in Al (see the previous paragraph). It should be noted, however, that for Al with high Zn concentration (30 wt.%) a part of the Zn content was segregated at the grain boundaries [25]. Fig. 3b shows Zn concentration profile across a grain boundary as obtained by energy dispersive X-ray spectroscopy (EDS) in transmission electron microscopy (TEM). It is evident that the grain boundary was enriched with Zn and the full width at the half maximum (FWHM) of the concentration profile is about 3 nm.

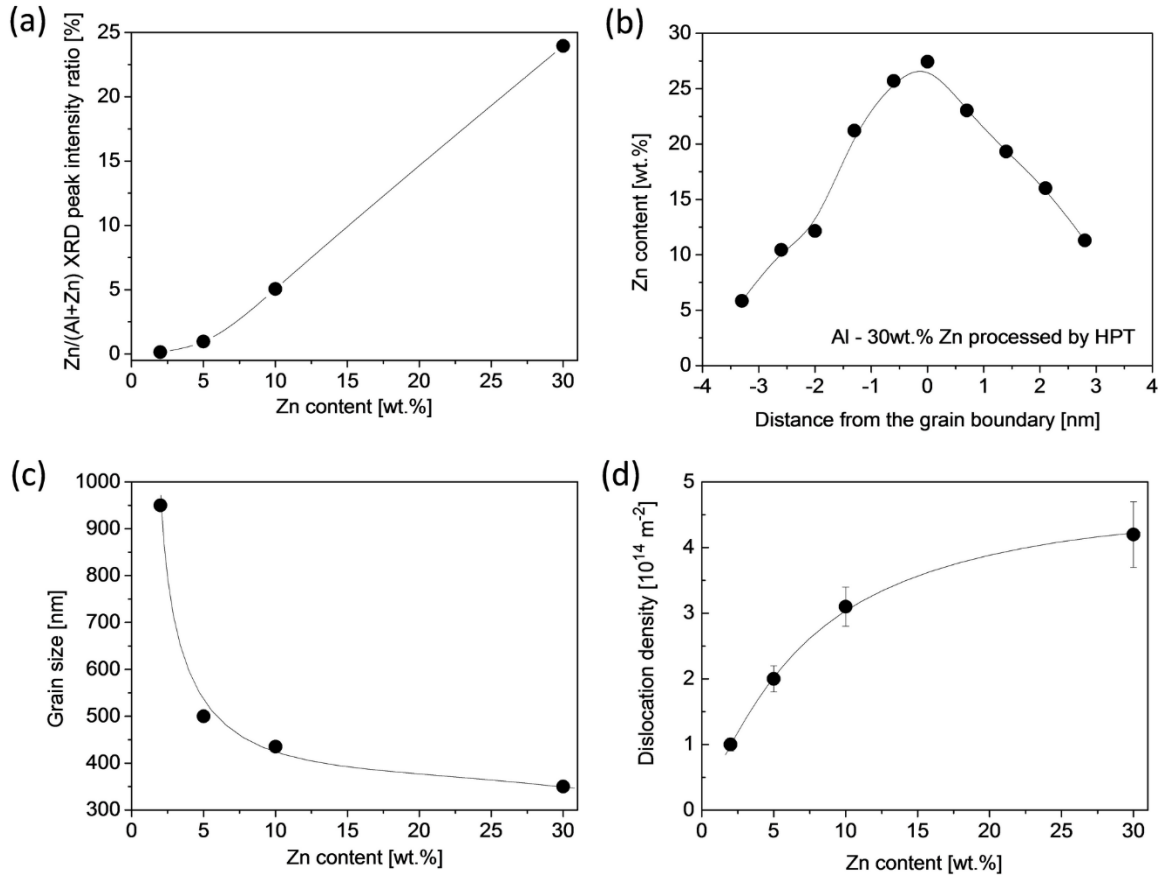

Figure 3. (a) The fraction of XRD intensity for the Zn phase versus the nominal Zn content in Al-Zn alloys processed by HPT until saturation. (b) The Zn content obtained by EDS in TEM as a function of the distance from a grain boundary in Al-30wt.%Zn alloy processed by HPT until saturation. (c) and (d) The grain size and the dislocation density, respectively, as a function of the nominal Zn content in Al-Zn alloys processed by HPT until saturation. The data were taken from [25].

The Zn content in Al processed by HPT has a significant effect on the microstructure of the Al phase. The average size of the Al grains decreased with increasing Zn content as can be seen in Fig. 3c. For the highest Zn concentration (30 wt.%) the grain size was refined to about 350 nm as determined by TEM [25]. The TEM images also revealed that the particles of the Zn phase can be found both in the triple junctions and the interiors of the Al grains. The size of the Zn particles inside the Al grains (5-15 nm) was much smaller than that in the triple junctions (100-200 nm). For low Zn concentrations, only small Zn particles in the grain interiors were observed. The dislocation density in the major Al phase was determined by X-ray diffraction line profile analysis [30]. Fig. 3d shows that the dislocation density increased monotonously with the Zn content. For the lowest (2 wt.%) and the highest (30 wt.%) nominal Zn concentrations, the dislocation density values were about 10^{14} m^{-2} and 4×10^{14} m^{-2}, respectively.

Fig. 4a shows the average hardness versus the nominal Zn content for the saturation state of the HPT-processed Al-Zn alloys [25]. For comparison, the hardness of the initial coarse-grained counterparts are also plotted. For low Zn concentrations ($\leq$ 5 wt.%), the hardness was enhanced with a factor of about two due to HPT which can be attributed to the increase of the dislocation density. For the sample containing 10 wt.% Zn, this factor is lower, and in the case of the Al-30wt.% Zn alloy considerable softening was observed after HPT despite the fact that the highest dislocation density was formed in this material. In this case, the deformation-softening can be explained by the decomposition of the initial supersaturated microstructure and the increased role of grain boundary sliding during hardness testing since the occurrence of this mechanism requires lower stress than that for dislocation glide inside the grains. The dominance of grain boundary sliding in Al-30wt.% Zn alloy can be attributed to the increased amount of grain boundaries due to the small grain size and the formation of a Zn-rich layer in the grain boundaries. The latter effect can facilitate grain boundary sliding as the diffusivity of Zn atoms along Al/Al grain boundaries is high [25], thereby resulting in an easier plasticity (i.e., softening).

It should be noted that the dominance of grain boundary sliding during plastic deformation is often accompanied by a large ductility or even superductility. A large ductility can be achieved if the strain rate sensitivity of the material is high (0.2-0.5). Fig. 4b shows the strain rate sensitivity for the HPT-processed Al-Zn alloys determined by indentation creep technique [31] as a function of the nominal Zn content. A monotonous increase of the strain rate sensitivity with the Zn content can be observed and for UFG Al-30wt.% Zn alloy the value of the strain rate sensitivity became relatively high, suggesting the dominance of grain boundary sliding in accordance with the deformation softening shown in Fig. 4a.

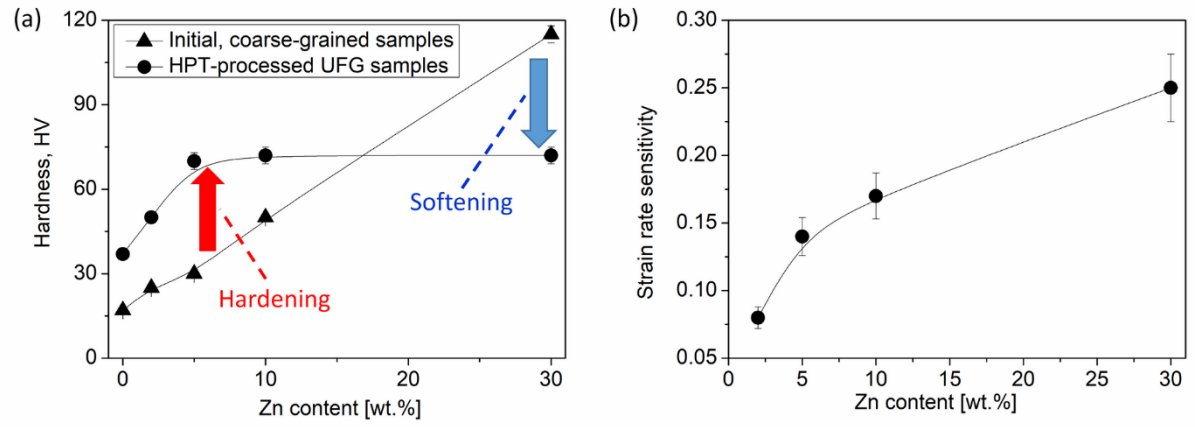

Figure 4. The hardness (a) and the strain rate sensitivity (b) versus the nominal Zn content in Al-Zn alloys processed by HPT until saturation. The data were taken from [25].

Deformation-softening was also detected in UFG Zn–22%Al and Zn–22%Al–0.3%Cu alloys with a duplex microstructure, i.e., in the material Al(Zn) and Zn(Al) solid solution phases coexisted [20]. Both

phases had similar grain sizes of 300-400 nm. This microstructure formed during aging of a solution treated alloy at RT. The hardness values of the aged UFG Zn–22%Al and Zn–22%Al–0.3%Cu alloys were 400 and 900 MPa, respectively. Then, these materials were subjected to rolling at RT up to the thickness reduction of 90% which corresponds to an equivalent strain of 2.3. This deformation caused a decrease of the hardness from 400 to 200 MPa for the Zn–22%Al sample while from 900 to 450 MPa for the Zn–22%Al–0.3%Cu alloy. The grain size did not change during this rolling, however the character of grain boundaries was significantly altered since dislocations and vacancies were accumulated in the grain boundaries. This change may cause an easier grain boundary sliding, thereby resulting in the observed softening at RT.

4. Deformation-softening caused by the decay of the dense lattice defect structure

Nanocrystalline and UFG materials processed by bottom-up techniques often have microstructures with a very high density of lattice defects such as dislocations and twin faults. A part of these grown-in defects can disappear from the microstructure during plastic deformation of the as-processed samples. This effect was demonstrated on electrodeposited nanotwinned Cu and Ni alloys [32-34]. It was shown that cold rolling resulted in softening due to the decrease of the density of growth dislocations and twin faults. This reduction of defect density can be caused by recovery, detwinning or recrystallization. In the first two processes, the dislocations formed during plastic deformation interact with the growth dislocations and twin faults leading to their decay, while in the last process new defect-free grains are nucleated, leading to softening.

5. Summary and conclusions

This paper overviewed the existing knowledge on deformation-softening for UFG materials. It was found that this effect may occur during plastic deformation of UFG samples which were formerly annealed at moderate homologous temperatures for short times. The applied heat treatment can cause the annihilation of mobile dislocations, leading to anneal-hardening. Then, subsequent plastic deformation can create new mobile dislocations, thereby resulting in softening.

Deformation softening can also be observed in UFG materials having low melting points (e.g., Sn, Pb, Zn and In), processed by SPD at RT. In these samples, due to the grain size reduction the main deformation mechanism changes from dislocation glide in the grain interior to grain boundary sliding. As the latter mechanism requires lower stress, softening was detected. For Al having larger melting temperature, softening due to room temperature SPD can be observed only if the purity level is 6N or higher. In this case, the possible occurrence of grain boundary sliding and the high mobility of dislocations are the main reasons of deformation-softening. The very low impurity content leads to an elevated mobility of dislocations which then can be annihilated very easily at the grain boundaries in the SPD-refined microstructure.

It should be noted that deformation-softening was also detected in Al-Zn alloy with elevated Zn content (30 wt.%). In this case, a Zn layer was formed on the Al/Al grain boundaries which facilitates grain boundary sliding due the enhanced diffusivity of Zn along these boundaries.

The as-grown lattice defect structures in nanomaterials processed by bottom-up methods such as electrodeposition can be decayed during severe plastic straining by recovery, detwinning or recrystallization, resulting in deformation-softening.

Acknowledgements

This research was supported by the Hungarian-Russian bilateral Research program (TÉT) No. 2017-2.3.4-TÉT-RU-2017-00005. This work was financed partly by the Ministry of Human Capacities of Hungary within the ELTE University Excellence program (1783-3/2018/FEKUTSRAT).

References

[1] Kovács I and Zsoldos L 1973 *Dislocations and Plastic Deformation* (Pergamon Press, Oxford)
[2] Gubicza J, Chinh NQ, Krállics Gy, Schiller I and Ungár T 2006 *Curr. Appl. Phys.* **6** 194
[3] Valiev RZ, Zhilyaev AP, Langdon TG 2014 *Bulk Nanostructured Materials, Fundamentals and Applications* (John Wiley & Sons, Inc., Hoboken, New Jersey)
[4] Gubicza J 2017 *Defect Structure and Properties of Nanomaterials* (Woodhead Publishing, Duxford, UK)
[5] Huang X, Hansen N and Tsuji N 2006 *Science* **312** 249
[6] Chinh NQ, Szommer P, Horita Z and Langdon TG 2006 *Adv. Mater.* **18** 34
[7] Valiev RZ, Sergueeva AV and Mukherjee AK 2003 *Scripta Mater*. **49** 669
[8] Zeng W, Shen Y, Zhang N, Huang X, Wang J, Tang G and Shan A 2012 *Scripta Mater*. **66** 147
[9] Atwater MA, Bahmanpour H, Scattergood RO and Koch CC 2013 *J. Mater. Sci*. **48** 220
[10] Volkov AY and Kliukin IV 2015 *Mater. Sci. Eng. A* **56** 627
[11] Gubicza J, Pereira PHR, Kapoor G, Huang Y, Subramanya Sarma V and Langdon TG 2018 *Adv. Eng. Mater.* **20** 1800184
[12] Wang YM, Cheng S, Wei QM, Ma E, Nieh TG and Hamza A 2004 *Scripta Mater*. **51** 1023
[13] Hasnaoui A, Van Swygenhoven H and Derlet PM 2002 *Acta Mater*. **50** 3927
[14] Valiev RZ, Enikeev NA, Murashkin MY, Kazykhanov VU and Sauvage X 2010 *Scripta Mater*. **63** 949
[15] Vo NQ, Schafer J, Averback RS, Albe K, Ashkenazy Y and Bellon P 2011 *Scripta Mater*. **65** 660
[16] Huang X 2009 *Scripta Mater.* **60** 1078
[17] Lee DH, Lee JA, Zhao Y, Lu Z, Suh JY. Kim JY, Ramamurty U, Kawasaki M, Langdon TG and Jang J 2017 *Acta Mater.* **140** 443
[18] Lee SW, Han SM and Nix WD 2009 *Acta Mater.* **57** 4404
[19] Liu FX, Liu ZL, Pei XY, Hu JQ and Zhuang Z 2017 *Int. J. Plasticity* **99** 102
[20] Yang CF, Pan JH and Lee TH 2009 *J. Alloy. Compd.* **468** 230
[21] Edalati K and Horita Z 2011 *Mater. Sci. Eng. A* **528** 7514
[22] Srinivasarao B, Zhilyaev AP, Langdon TG and Perez-Prado MT 2013 *Mater. Sci. Eng. A* **562** 196
[23] Edalati K, Cubero-Sesin JM, Alhamidi A, Mohamed IF and Horita Z 2014 *Mater. Sci. Eng. A* **613** 103
[24] Ito Y, Edalati K and Horita Z 2017 *Mater. Sci. Eng. A* **679** 428
[25] Chinh NQ, Jenei P, Gubicza J, Bobruk EV, Valiev RZ and Langdon TG 2017 *Mater. Lett.* **186** 334
[26] Chinh NQ, Szommer P, Horita Z and Langdon TG 2006 *Adv. Mater.* **18** 34
[27] Kawasaki M 2014 J. Mater. Sci. **49** 18
[28] Kawasaki M, Figueiredo RB, Huang Y and Langdon TG 2014 *J. Mater. Sci.* **49** 6586
[29] Popovic S and Grzeta B 1999 *Croatica Chemica Acta* **72** 621
[30] Gubicza J 2014 *X-ray line profile analysis in Materials Science* (IGI-Global, Hershey, USA)
[31] Chinh NQ and Szommer P 2014 *Mater. Sci. Eng. A* **611** 333
[32] Ungár T, Li L, Tichy G, Pantleon W, Choo H and Liaw PK 2011 *Scripta Mater*. **64** 876
[33] Niu R and Han K 2013 *Scripta Mater*. **68** 960
[34] Ni HT, Zhu J and Zhang XY 2017 *J. Alloy. Compd* **693** 226